Supporting Material

"Modeling membrane deformations and lipid demixing upon protein-membrane interaction: The BAR dimer adsorption"

George Khelashvili, Daniel Harries, and Harel Weinstein

Parametrization of Membrane Shape

In this section we present the parametrization procedure for the membrane shape. Our description is based on the Monge representation where a position vector $\vec{r}$ of the bilayer upper or lower leaflets, or bilayer mid-plane (see Fig. $1B$ of the main text) is given by $\vec{r} \equiv (x, y, h(x, y))$. The height function $h(x, y)$ is the distance between the curved surface and the flat reference (x, y) plane. In the Monge gauge the metric of the surface is given by:

$$g_{ij} = \frac{\partial \vec{r}}{\partial u^i} \times \frac{\partial \vec{r}}{\partial u^j}, \qquad i, j = 1, 2 \tag{1}$$

where $u^1 \equiv x, u^2 \equiv y$. From Eq. 1

$$g \equiv |g_{ij}| = 1 + h_x^2 + h_y^2 \tag{2}$$

with $h_x \equiv \partial_x h(x, y)$ and $h_y \equiv \partial_y h(x, y)$. The area element of the curved surface is:

$$dA = \sqrt{g} dx dy = \sqrt{1 + h_x^2 + h_y^2} dx dy \tag{3}$$

and the Cartesian components of the local surface element normal unit vector $\vec{n} = (n_x, n_y, n_z)$ are given by:

$$n_x = \frac{-h_x}{\sqrt{g}} \tag{4}$$

$$n_y = \frac{-h_y}{\sqrt{g}} \tag{5}$$

$$n_z = \frac{1}{\sqrt{g}} \tag{6}$$

With that, one can derive for the local curvature:

$$c(x, y) = \frac{(1 + h_y^2) h_{xx} + (1 + h_x^2) h_{yy} - 2 h_x h_y h_{xy}}{2 g^{3/2}} \tag{7}$$

where $h_{xx} \equiv \partial_{xx} h(x,y)$, $h_{yy} \equiv \partial_{yy} h(x,y)$, and $h_{xy} \equiv \partial_{xy} h(x,y)$. Eq. 3 and Eq. 7 are used throughout the equations in the main text and in the Supporting Material.

Elements of membrane remodeling

In the transformation of a membrane that is spontaneously flat at equilibrium into a highly curved structure, BAR appears to take advantage of a special set of structural features. First, the electrostatic interactions between positively charged residues on BAR's concave surface and phospholipid headgroups may cause membrane deformations out of the bilayer plane, resulting in a pulling of the membrane towards, or away from the protein. The same electrostatic interactions may also cause lateral sequestration of charged phospholipids near the protein(1–7). This process of lipid demixing in the bilayer plane has been predicted to be particularly significant in membranes containing multivalent lipids, such as phosphatidylinositol 4,5-biphosphate (PIP_2) lipids(1, 3). Segregation of such highly charged lipids (net head-group charge of -4.0 at neutral pH(8)) would not only enhance the overall electrostatic interactions between BAR and membrane, but could lead as well to local asymmetry between the spontaneous curvatures of the two monolayers comprising a lipid membrane, simply because the head group of PIP_2 is larger than most mono-valent lipids, such as phosphatidylserine (PS) or zwiterionic lipids, like phosphatidylcholine (PC). Such asymmetry would be sufficient to produce a local "positive" curvature in the two *bilayer* leaflets, towards the BAR(9–11). Therefore, sequestering charged lipids could potentially lead to a new stable state, in which bilayer bending forces favor membranes with local non-zero curvature.

These components of the interaction energy are accounted for in the approach we describe here. Moreover, the mechanism for coupling local

lipid composition with membrane curvature may be complemented by a "local spontaneous curvature" mechanism (11), in which the asymmetry between the spontaneous shapes of two monolayers is achieved by insertion of amphipathic N-terminal helices of certain BAR domains into the lipids polar headgroups region(11–21). In this mechanism, the insertion of an amphipathic peptide into one of the leaflets of a flat membrane produces an increase in the local spontaneous curvature of that leaflet because of the local bending of the monolayer where the helix is embedded(9–11). Differences in the spontaneous curvatures of two monolayers comprising a lipid membrane establishes a new equilibrium state, in which, bilayer elastic forces support a locally curved membrane shape.

Free energy minimization

In this section we detail the free energy minimization procedure implemented to obtain an equilibrium state for BAR-membrane complex. Because the free energy functional F (Eq.(2) of the main text) contains electrostatic, mobile ion mixing, lipid mixing, and membrane bending energy contributions, F must be minimized with respect to all these relevant degrees of freedom in a self-consistent manner. In particular, minimization with respect to mobile ion concentrations leads to the non-linear Poisson-Boltzmann (PB) equation(22–28):

$$\nabla^2\Psi = \lambda_D^{-2}\sinh\Psi \tag{8}$$

Solving this equation yields the electrostatic potential Ψ.

In order to minimize the free energy functional with respect to the lipid compositional degrees of freedom, we use the Cahn-Hilliard (CH) formalism (29), carried out here as discussed in detail in Ref.(1). Briefly, according to the CH description, lipids diffuse in the membrane plane due to the local

gradients in their electrochemical potentials(30, 31), where the steady-state solution of the CH equations at long times is obtained self-consistently with the PB equation and corresponds to the lipid distribution that minimizes F with respect to all local lipid mole fractions. Thus, propagating local lipid compositions with these diffusion-like equations eliminates the need to tackle an additional 2D boundary condition on the membrane surface(1, 32, 33), which in general is easily solvable only for systems of high geometric symmetry.

In order to implement the CH formalism for a membrane composed of binary mixtures of charged and neutral lipids, we first use free energy functional expression (Eq.(2) of the main text) to derive the electrochemical potential of charged lipids on either leaflet as:

$$\mu = \mu^{\circ} + \frac{\partial F}{\partial N} = \mu^{\circ} + k_B T \left[\ln \frac{\phi(1-\phi^0)}{\phi^0(1-\phi)} + z\Psi \right] + a\kappa(c_n^0 - c_c^0)(c - c^0(\phi)) \quad (9)$$

Here N is the number of charged lipids on a single membrane layer, and μ° represents the standard chemical potential for the charged lipid species(that is independent of ϕ). The temporal evolution of the spatial charged-lipid compositions on both leaflets are linked to the Laplacians of the corresponding electrochemical potentials through the pair of CH equations:

$$\begin{aligned} \frac{\partial \phi_u(\vec{r},t)}{\partial t} &= \frac{D_{lip}}{k_B T} \nabla^2_{LB}(\mu_u) \\ \frac{\partial \phi_l(\vec{r},t)}{\partial t} &= \frac{D_{lip}}{k_B T} \nabla^2_{LB}(\mu_l) \end{aligned} \quad (10)$$

Here D_{lip} is the lipid diffusion coefficient that should not affect the equilibrium state, and the subscript LB denotes the Laplace-Beltrami operator (the analog of the Laplace operator on curved surfaces). The evolution of neutral lipids follows from the above equations taken together with the incompressibility relations. We stress that, in general, the CH equations are

implemented to describe time evolution of globally conserved fields. Here we do not intend to study dynamic aspects of lipid diffusion, but rather use Eqs. 10 and 9 for the sole purpose of minimizing the free energy functional F with respect to local lipid fractions. This is achieved by iteratively solving the resulting dimensionless CH equations for lipid compositions on the two leaflets:

$$\begin{aligned}\phi(\vec{r},t'+\Delta t') &= \phi(\vec{r},t') + \Delta t' \nabla'^2_{LB}\left[\ln\frac{\phi(\vec{r},t')(1-\phi^0)}{\phi^0(1-\phi(\vec{r},t'))} + z\Psi(\vec{r},t')\right] \\ &+ \Delta t' a' \kappa' (c_n^{0'} - c_c^{0'}) \nabla'^2_{LB}\left[c'(\vec{r},t') - c^{0'}(\phi(\vec{r},t'))\right]\end{aligned} \tag{11}$$

where we have used primed variables to denote the following unitless quantities:

$$t' = tD_{lip}/\xi^2; \qquad \kappa' = \kappa/k_BT; \qquad c' = c\xi; \qquad a' = a\xi^2 \tag{12}$$

where ξ is the lattice constant.

We also note that according to Eqs. 9 - 11, lipids may locally demix not only due to electrostatic interactions with the protein but also due to their tendency to preferentially form different spontaneous shapes. As an example, monovalent acidic PS, or poly-valent PIP_2 lipids have inherent positive spontaneous curvature at neutral pH(11), and therefore are expected to associate into positively curved membrane regions. Neutral PC lipids, on the other hand, would prefer negatively curved membrane patches(11). Therefore, it is obvious that an additional minimization of the free energy functional with respect to membrane shape is necessary and that the procedure should be carried out self-consistently together with the electrostatic and repulsive interactions, as well as with lipid mixing. This presents a formidable challenge, since in principle one has to consider all possible changes in membrane geometry, and couple these shape deformations to other degrees of

freedom.

Here, the combined scheme is used to efficiently account for bilayer deformations and self-consistently with the PB equation; together with the CH equations the method converges to the (local) minimum of the total free energy. Our strategy is based on representing the membrane shape as a linear superposition of Gaussian functions (used here as a basis set). With that, we sample membrane deformations by varying only the Gaussian amplitudes. This procedure significantly reduces the dimensionality of phase space that needs to be explored. The Gaussian's amplitudes are varried randomly, and trial moves are accepted if the free energy is reduced. To ensure self-consistency, at each trial move we solve the PB equation for the electrostatic potential. To couple shape changes to lipid demixing, we alternate the steps for membrane deformations with the CH moves for local lipid compositions. The outline of the algorithm can be found in the next section.

In several calculations reported in Results we make the simplifying assumption that the lipid composition within a membrane patch is constant and homogeneous. In such cases, there is no need to solve the CH equations for local lipid fractions, and our minimization scheme reduces to performing random moves for local membrane heights self-consistently with solving electrostatic problem. In addition, when we discuss homogeneous mixtures (no lipid segregation), we conveniently express elastic properties of the membrane per *bilayer* and describe membrane geometry with respect to the bilayer mid-plane(see Fig.1*B*)(34, 35). In particular, we assume that the bending modulus of the bilayer $\kappa = 2\kappa_m$(34–36), and we denote the spontaneous curvature of the bilayer mid-plane by c_0. Then the elastic free energy expression in Eq.(6) of the main text simplifies to: $F_b = \frac{1}{2}\kappa \int_{A_m} dA_m (c_m - c_0)^2$(34, 35), where c_m is the local curvature of the

mid-plane and the integration is carried out over the bilayer mid-plane surface.

To introduce the N-helix membrane interaction in our model, an additional energy term must be added to the free energy functional (Eq.(2) of the main text) in a manner similar to the work in Ref.(9, 10), and the coupling between peptide insertion and BAR interaction must be considered in the self-consistent form adopted in the model. However, the nature of the coupling among these degrees of freedom is not known, which makes the formulation of a free energy functional that can couple the electrostatic and elastic degrees of freedom that will also include peptide insertions quite challenging. Here we use a simplified approach to couple the N-helix inclusions to the electrostatic contributions, by modeling insertion effects implicitly. Thus, we define a locally positive spontaneous curvature region on the bilayer adjacent to the adsorbing BAR domain (shown in Fig. 3 of the main text), and use a phenomenological approach that assumes that the inclusions (two insertions per BAR dimer) perturb the bilayer asymmetry and its elastic properties primarily around the area of insertion(9). We account for insertions at different depths by varying the value for the spontaneous curvature assigned to this local membrane region(10). For each insertion depth, the bilayer adjusts its geometry locally, and the deformations at steady state for each penetration depth is found by minimizing the modified free energy functional which now contains an elastic free energy term that accounts for the non-zero spontaneous curvature region near the adsorbed BAR dimer.

Basic steps in the free energy minimization algorithm

In this section we detail the basic steps in the free energy minimization algorithm. Our method is based on the idea that any two-dimensional surface

shape can be represented by a linear combination of a suitable set of analytical functions, called the basis set(see for example (37, 38)). One common choice, used here, is the basis set of Gaussian functions(38). Imagine N two-dimensional Gaussians centered at different locations and each having the following functional form:

$$g_i(x,y) = A_i \times \exp\left[-\left(\frac{(x-x_i^0)^2}{\sigma_{xi}^2} + \frac{(y-y_i^0)^2}{\sigma_{yi}^2}\right)\right], \qquad i = 1, ...N. \quad (13)$$

where the *i-th* Gaussian is centered at (x_i^0, y_i^0), and its amplitude and two variances, along x and y directions, are A_i, σ_{xi} and σ_{yi} respectively. Then the height with respect to a flat reference plane of the bilayer mid-surface at point (x,y) can be approximated as a linear superposition of these Gaussian functions:

$$h(x,y) \approx \sum_{i=1}^{N} g_i(x,y) \quad (14)$$

Eq. 14 becomes exact as $N \to \infty$. The advantage here is that, with a careful choice of N and all (x_i^0, y_i^0)-s (see the next section, Simulation Details), it becomes sufficient to systematically vary only the Gaussian's amplitudes and variances in order to efficiently sample membrane deformations. This procedure significantly reduces the dimensionality of the phase space one has to explore. To further simplify calculations, we set σ_x and σ_y variances of all N Gaussians to be identical and fixed, so that we perform the sampling procedure only on the Gaussian's amplitudes.

The algorithm starts with designing a membrane mid-surface of certain initial geometry using Eqs. 13 and 14. With parallel translation, we obtain the locations of the two charged surfaces: the upper and lower leaflets(see Fig. $1B$ of the main text). We then place the desired number of lipids in both leaflets by creating suitable charge densities on the two layers; usually we start with a homogeneous distribution of lipids on both leaflets. With

the membrane geometry fixed, the BAR dimer is positioned in the desired orientation near the membrane, and Cahn-Hilliard moves are performed to vary the local lipid compositions(1), and to achieve lipid demixing under the influence of the electrostatic forces from the BAR and the elastic forces, which act to locally separate lipids according to their spontaneous curvature values. To achieve self-consistency, the non-linear PB equation is solved after each CH step to update the electrostatic potential in space. This iterative process is repeated until significant lipid segregation is observed(1), usually for 300-400 steps, depending on the lipid content.

Then, we fix the lipid composition and perform trial moves on the membrane shape by executing the following steps:

1) With the BAR fixed in the same orientation as during the CH procedure, solve the non-linear PB equation.

2) The electrostatic, bending, lipid mixing and repulsive energy contributions are calculated to obtain the adsorption free energy of the BAR-membrane complex:

$$\Delta F_{old} = F^{old}_{complex} - F_{reference} \tag{15}$$

Here $F^{old}_{complex}$ is the total free energy of the complex, and $F_{reference}$ is the total free energies of the BAR-membrane reference state.

3) Randomly pick the i-th Gaussian, and attempt to change its amplitude $A^{new}_i = A^{old}_i + \Delta r$, where Δr is a uniform random number in the range [-1;1].

4) Using the updated list of Gaussian amplitudes, construct a trial configuration of the bilayer mid-surface and upper and lower leaflets.

5) Position BAR as in step 1 next to the trial membrane and calculate the adsorption free energy of the BAR-membrane complex, ΔF_{new}. Note that the lipid composition does not change between old and trial configurations.

6) If $\Delta F_{new} \leq \Delta F_{old}$, accept the trial configuration of the membrane

and go to step 3. If $\Delta F_{new} > \Delta F_{old}$, discard the trial configuration and go to step 3.

Steps 3-6 are repeated until the membrane locally adopts its shape with respect to particular existing lipid distribution. Then, fixing the membrane geometry, we again perform Cahn-Hilliard iterations to relax the local lipid compositions, which is followed by trial steps for varying bilayer shape.

The entire loop is repeated multiple times and convergence of the algorithm to equilibrium is verified by confirming that there is no change, within numerical uncertainty, in the adsorption free energy with additional steps. Because in the algorithm the system is driven along a free energy gradient, it is tacitly assumed here that the balance of bending, electrostatic, lipid mixing and repulsive contributions exists only in one particular configuration, i.e. that the landscape of the free energy functional as defined in Eq.2 of the main text has only a single minimum. The validity of this assumption is supported by our test calculations with different initial membrane shapes. Thus, we performed the minimization procedure on BAR/membrane systems where the membrane was initially either flat or had substantial spherical deformation in the region near the adsorbed BAR. The results indicated that both starting points converged to the same final structure, however we found that the convergence from the pre-formed spherical configuration was faster. Therefore, we used membranes with pre-formed spherical domes as the initial starting point for all the simulations reported here.

We also note that any change in membrane shape will be accompanied by change in number of lipids in the simulation cell. In order to maintain a constant charge density on the two leaflets, we imagine the simulation box being coupled to a large lipid reservoir that can constantly exchange lipids with the central cell. Accordingly, at each of shape perturbation we correct the free energy functional in Eq.2 of the main text by the standard term

$\Delta f = -\Delta N \times f_{bulk}$(39), where $\Delta N = N_{new} - N_{old}$ is the difference in lipid number in the trial and current states, and f_{bulk} is the free energy per lipid in the bulk membrane (away from the adsorbed BAR).

Simulation details

We consider here the BAR domain from the Amphiphysin protein (PDB ID code 1URU) and represent it in full-atomistic 3D details, by assigning to each atom a radius and a partial charge. This BAR module contains 12 positive residues along its concave surface, and thus is characterized by a higher charge density on the membrane-facing side as compared with other BAR domains (see Fig.1 of the main text)(12).

The BAR is fixed in space near the membrane in an orientation with its long axis parallel to the flat membrane's (x,y) plane, and the short axis perpendicular to that plane (along z) as depicted in Fig. 1B. Calculations for different BAR orientations revealed that such positioning of the BAR next to membranes compared to any tilted orientation resulted in the most favorable binding free energies and largest membrane deformations (data not shown). We do not explicitly consider the amphiphatic N-terminal helices of the BAR domain, but instead, model the effects of the N-helical insertions implicitly through their effect on the membrane elastic properties.

We focus on lipid membranes of 30:70 PS/PC ($\phi = 0.3$), and 4:96 PIP_2/PC ($\phi = 0.04$) average compositions. Assuming an area per lipid headgroup of a=65Å^2 for all lipids, these mixtures correspond to charge densities of $\sigma \sim -0.004e$ and $\sigma \sim -0.0025e$ respectively. Our choices of membrane compositions are motivated by the following: 1) 30:70 PS/PC is a biologically relevant composition that mimicks the model membrane used in atomsitic simulations by Blood et al (40, 41); 2) The average composi-

tional range of PIP_2 lipids is known to be 1%-5% (8). In agreement with experimental observations (3), we have recently demonstrated(1) that, as charged proteins diffuse on a 75:24:1 PC/PS/PIP_2 membrane, they primarily sequester PIP_2 lipids, whereas the PS lipid distribution remains largely uneffected by the adsorbed protein. Thus, exploring PS- vs. PIP_2-containing mixtures enables us to specifically address the role of lipid sequestration in the process of membrane remodeling by BAR domains. To make numerical calculations simpler, we consider here both model membranes as binary mixtures of both 4:96 PIP_2/PC and 30:70 PS/PC.

The spontaneous curvatures of PS and PC lipids were set to c^0_{PS}=1/144 Å^{-1} and c^0_{PC}=-1/100 Å^{-1} respectively, values that were also reported in the literature(11, 42–44). The spontaneous curvature of PIP_2 lipid is not known from experimental measurements. We assume here $c^0_{PIP_2}$=1/70 Å^{-1}, in light of the substantial difference in head group size between PIP_2 and monovalent PS.

For all calculations the lipid membrane was modeled as a low dielectric slab ($\epsilon_m = 2$) of dimensions 256Å $\times$ 256Å $\times$ 40Å. Electrostatic calculations were performed using a modified version of the publicly available open source software: APBS version 0.4.0(45). The system was placed on a 256Å $\times$ 256Å $\times$ 256Å cubic grid with grid spacing of 1Å, and the non-linear PB was discretized with the finite-difference method. The APBS software was modified to include periodic boundary conditions in the (xy) bilayer in-plane directions. The charge, ion accessibility, and dielectric maps were configured and supplied to APBS. After each MC or CH step in the free energy minimization procedure, these maps were updated and fed back to the PB solver to obtain new electrostatic potential.

The periodic box contained 1:1 electrolyte solution of n_0 =0.1M concen-

tration, corresponding to a Debye length of $\lambda_D \approx 10$Å:

$$\lambda_D = \left(\frac{\epsilon_0 \epsilon_w k_B T}{2e^2 n_0} \right)^{1/2} \tag{16}$$

Here k_B is Boltzmann's constant, T=300K - the temperature, e - the elementary charge, ϵ_0 - the permeability of free space, and $\epsilon_w = 80$ is the dielectric constant of the aqueous solution.

As a basis set for the minimization procedure, we chose N=841 Gaussians placed equidistant from each-other on a two-dimensional (x,y) grid 9Å apart. The variances σ_x and σ_y for all Gaussians were taken as 20Å. This setup not only ensured complete coverage of the membrane surface by the Gaussians, but also provided strong overlap between neighboring Gaussian functions and made the minimization scheme efficient. Further, we used the intrinsic 2-fold symmetry of the BAR domain so that step 3 in the Monte Carlo algorithm (see previous section) was carried out simultaneously and in an identical manner on two symmetrically situated Gaussians.

The free energy minimization cycles were performed repeatedly until we observed no change, within numerical uncertainty, in the adsorption free energy with additional steps, implying no changes in lipid distribution and in membrane shape with further iterations.

References

1. Khelashvili, G., H. Weinstein, and D. Harries. 2008. Protein Diffusion on Charged Membranes: A Dynamic Mean-Field Model Describes Time Evolution and Lipid Reorganization. *Biophys. J.* 94:2580-2597.

2. Wang. J., A. Gambhir, G. Hangyas-Mihalyne, D. Murray, U. Golebiewska, and S. McLaughlin. 2002. Lateral sequestration of phosphatidylinositol 4,5-biphosphate by the basic effector domain of mystoylated alanine-rich C Kinase substrate is due to nonspecific electrostatic interactions. *J. Biol. Chem.* 277:34401-34412.

3. Golebiewska, U., A. Gambhir, G. Hangyas-Mihalyne, I. Zaitseva, J. Radler, and S. McLaughlin. 2006. Membrane-Bound basic peptides sequester multivalent (PIP_2), but not monovalent (PS), acidic lipids. *Biophys. J.* 91:588-599.

4. Haleva, E., N. Ben-Tal, and H. Diamant. 2004. Increased concentration of polyvalent phospholipids in the adsorption domain of a charged protein. *Biophys. J* 86:2165-2178.

5. Wang J. A. Gambhir, S. McLaughlin, and D. Murray. 2004. A computational model for the electorstatic sequestration of $PI(4,5)P_2$ by membrane-adsorbed based peptides. *Biophys. J.* 86:1969-1986.

6. McLaughlin, S., and D. Murrray. 2005. Plasma membrane phosphoinositide organization by protein electrostatics. *Nature* 438:605-611.

7. Tzlil, S., and A. Ben-Shaul. 2004. Increased concentration of polyvalent phospholipids in the adsorption domain of a charged protein. *Biophys. J.* 89:2165-2178.

8. McLaughlin, S., J. Wang, A. Gambhir, and D. Murray. 2002. PIP_2 and proteins: interactions, organization, and information flaw. *Annu. Rev. Biophys. Struct.* 31:151-75.

9. Zemel, A., A. Ben-Shaul, and S. May. 2005. Pertrubation of a lipid membrane by amphiphatic peptides and its role in pore formation. *Eur. Biophys. J.* 34:230-242.

10. Campelo, F., H.T. McMahon, and M. M. Kozlov. 2008. The hydrophobic insertion mechanism of membrane curvature generation by proteins. *Biophys. J.* 95:2325-2339.

11. Zimmerberg, J., and M. M. Kozlov. 2006. How proteins produce cellular membrane curvature. *Nature Reviews: Mol. Cell. Biol.* 7:9-19.

12. Peter, B. J., H. M. Kent, I. G. Mills, Y. Vallis, P. J. G. Butler, P. R. Evans, and H. T. McMahon. 2004. BAR domains as sensors of membrane curvature: the Ampiphysin BAR structure. *Science* 303:495-499.

13. Gallop, J. L., and H. T. McMahon. 2005. BAR domains and membrane curvature: bringing your curves to the BAR. *Biochm. Soc. Symp.* 72:223-231.

14. Itoh, T., and P. De Camilli. 2006. BAR, F-BAR (EFC) and ENTH/ANTH domains in the regulation of membrane-cytosol interfaces and membrane curvature. *BBA* 1761:897-912.

15. Gallop, J. L., C. C. Jao, H. M. Kent, P. J. G. Butler, P. R. Evans, R. Langen and H. T. McMahon. 2004. Mechanism of endophilin N-BAR domain-mediated membrane curvature. *EMBO* 25:2898-2910.

16. Farsad, K., N. Ringstad, K. Takei, S. R. Floyd, K. Rose, and P. De

Camilli. 2001. Generation of high curvature membranes mediated by direct endophilin bilayer interactions. *JCB* 155(2):193-200.

17. Masuda, M., S. Takeda, M. Sone, T. Ohki, H. Mori, Y. Kamioka, and N. Mochizuki. 2006. Endophilin BAR domain drives membrane curvature by two newly identified structure-based mechanisms. *EMBO* 25:2889-2897.

18. Ford, M. G. J., I. G. Mills, B. J. Peter, Y. Valls, G. J. K. Praefcke, P. R. Evans, and H. T. McMahon. 2002. Curvature of clathrin-coated pits driven by epsin. *Nature* 419:361-366.

19. Lee, M. C. S., L. Orci, S. Hamamoto, E. Futal, M. Ravazzola, and R. Schekman. 2005. Sar1p N-terminal helix initiates membrane curvature and completes the fission of a COPII vesicle. *Cell* 122:605-617.

20. Nie, Z., D. S. Hirsch, R. Luo, X. Jian, S. Stauffer, A. Cremesti, J. Andrade, J. Lebowitz, M. Marino, B. Ahvazi, J. E. Hinshaw, and P. A. Randazzo. 2006. A BAR domain in the N terminus of the Arf GAP ASAP1 affects membrane structure and trafficking of epidermal growth factor receptor. *Curr. Biol.* 16:130-139.

21. Fernandes, F., L. M. S. Loura, F. J. Chichon, J. L. Carrascosa, A. Fedorov, and M. Prieto. 2008. Role of Helix-0 of the N-BAR domain in membrane curvature generation. *Biophys. J.* 94:3065-3073.

22. Sharp, K. A., and B. Honig. 1990. Electrostatic interactions in macromolecules: theory and applications. *Annu. Rev. Biophys. Chem* 19:301-32.

23. Andelman, D. 1995. Electrostatic properties of membranes: The Poisson-Boltzmann theory. 1B 603-642. Handbook of Biological Physics. Elsevier Science B.V., Amsterdam.

24. Reiner, E.S., and C.J. Radke. 1990. Variational approach to the electrostatic free energy in charged colloidal suspensions: general theory for open systems. *J. Chem. Soc., Faraday Trans.* 86:3901-3912.

25. Honig, B., and A. Nicholls. 1995. Classical electrostatics in Biology and Chemistry. *Science.* 268:1144-1149.

26. Borukhov, I., D. Andelman, and H. Orland. 1997. Steric Effects in Electrolytes: A Modified Poisson-Boltzmann Equation. *Phys. Rev. Lett.* 79:435-438.

27. Fogolari, F., and J. M. Briggs. 1997. On the variational approach to the Poisson-Boltzmann free energies. *Chem. Phys. Lett.* 281:135-139.

28. Murray, D., A. Arbuzova, B. Honig, and S. McLaughlin. 2002. The role of electrostatic and nonpolar interactions in the association of peripheral proteins with membranes. *Current Topics in Membranes.* Volume 52. Chapter 10. pp:277-307.

29. Chaikin, P.M. and T.C. Lubensky, 2000. Principles of Condensed Matter Physics. Cambridge university press, Cambridge.

30. Chandrasekar, S. 1943. Stochastic problems in physics and astronomy. *Rev. Mod. Phys.* 15:1-89.

31. Krishna, R., and J. A. Wesselingh. 1997. The Maxwell-Stefan approach to mass transfer. *Chem. Engin. Sci.* 52:861-911.

32. Harries, D., S. May, and A. Ben-Shaul. 2003. Curvature and charge modulations in lamellar DNA-lipid complexes. *J. Phys. Chem. B.* 107:3624-3630.

33. May, S., D. Harries, and A. Ben-Shaul. 2000. Lipid demixing and protein-protein interactions in the adsorption of charged proteins on mixed membrane. *Biophys. J.* 79:1747-1760.

34. Siegel, D. P., and M. M. Kozlov. 2004. The Gaussian Curvature Elastic Modulus of N-Monomethylated Dioleoylphosphatidylethanolamine: Relevance to Membrane Fusion and Lipid Phase Behavior *Biophys. J.* 87:366 - 374.

35. Marsh, D. 2006. Elastic curvature constants of lipid monolayers and bilayers. *Chem. Phys. Lip.* 144:146-159.

36. Petrache, H. I., D. Harries, and V. A. Parsegian. 2005. Alteraion of lipid membrane rigidity by cholesterol and its metabolic precursors. *Macromol. Symp.* 219:39-50.

37. Davidson, E. 1986. Basis set selection for molecular calculations. *Chem. Rev.* 86(4):681-696.

38. Leach, A. 1996. Molecular modelling: principle and applications. Singapore: Longman.

39. Harries, D., and V. A. Parsegian. 2004. Gibbs adosption isotherm combined with Monte Carlo sampling to see the action of cosolutes on protein folding. *Proteins* 57:311-321.

40. Blood, P. D., and G. A. Voth. 2006. Direct observation of Bin/amphiphysin/Rvs (BAR) domain-induced membrane curvature by means of molecular dynamics simulations. *PNAS* 103(41):15068-15072.

41. Blood, P. D., R. D. Swenson, and G. A. Voth. 2008. Factors infuencing local membrane curvature induction by N-BAR domains as revealed by molecular dynamics simulations. *Biophys. J.* 95:1866-1876.

42. Fuller, N., Benatti, C.R., and Rand, R.P. 2003. Curvature and bending constants for phosphatidelserine-containing membranes. *Biophys. J.* 85:1667-1674.

43. Chen, Z., and Rand, R.P. 1997. The influence of cholesterol on phospholipid membrane curvature and bending elasticity. *Biophys. J.* 73:267-276.

44. Szule, J. A, Fuller, N.L., and Rand, R.P. 2002. The effects of acyl chain length and saturation of diacylglycerols and phophatidylcholines on membrane monolayer.*Biophys. J.* 83:977-984.

45. Baker, N. A., D. Sept, S. Joseph, M. J. Holst, and J. A. McCammon. 2001. Electrostatics of nanosystems: application to microtubules and the ribosome. *Proc. Natl. Acad. Sci. USA* 98:10037-10041.

Figure Captions

Figure S1. Adsorption of the Amphiphysin BAR domain on membranes of $\sigma = -0.004e/\text{Å}^2$ average surface charge density ($\phi^0_{PS} = 0.3$) and with preformed spherical deformation. The variation in the binding free energy (in k_BT units) is shown versus the radius of the spherical cap. Inset depicts the BAR (in ball-and-stick representation) adsorbed onto a membrane deformed into a spherical cap of R=100 Å (green). We show only the portion of the membrane's upper leaflet neighboring the BAR, close to the spherical deformation. The membrane shape smoothly transitions to the flat state in the bulk.

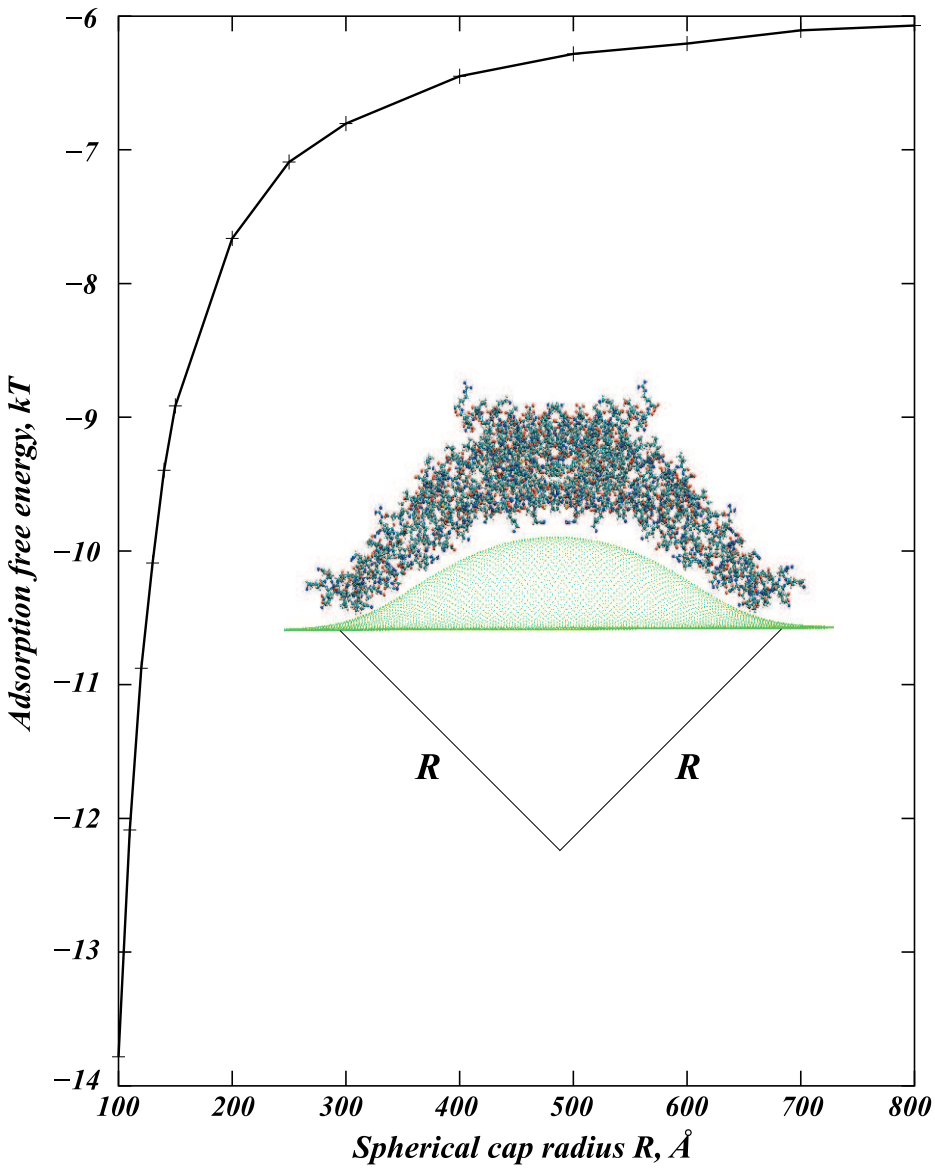

Figure S1 **(GK, HW and DH)**